Maximum entropy snapshot sampling for reduced basis modelling

Marcus W.F.M. Bannenberg
IMACM, Bergische Universität Wuppertal, Chair of Applied Mathematics and Numerical Analysis (AMNA), Wuppertal, Germany and STMicroelectronics, Catania, Italy

Fotios Kasolis
IMACM, Bergische Universität Wuppertal, Chair of Electromagnetic Theory, Wuppertal, Germany

Michael Günther
IMACM, Bergische Universität Wuppertal, Chair of Applied Mathematics and Numerical Analysis (AMNA), Wuppertal, Germany, and

Markus Clemens
STMicroelectronics, Catania, Italy

Received 19 February 2021
Revised 8 July 2021
Accepted 7 September 2021

Abstract

Purpose – The maximum entropy snapshot sampling (MESS) method aims to reduce the computational cost required for obtaining the reduced basis for the purpose of model reduction. Hence, it can significantly reduce the original system dimension whilst maintaining an adequate level of accuracy. The purpose of this paper is to show how these beneficial results are obtained.

Design/methodology/approach – The so-called MESS method is used for reducing two nonlinear circuit models. The MESS directly reduces the number of snapshots by recursively identifying and selecting the snapshots that strictly increase an estimate of the correlation entropy of the considered systems. Reduced bases are then obtained with the orthogonal-triangular decomposition.

Findings – Two case studies have been used for validating the reduction performance of the MESS. These numerical experiments verify the performance of the advocated approach, in terms of computational costs and accuracy, relative to gappy proper orthogonal decomposition.

Originality/value – The novel MESS has been successfully used for reducing two nonlinear circuits: in particular, a diode chain model and a thermal-electric coupled system. In both cases, the MESS removed unnecessary data, and hence, it reduced the snapshot matrix, before calling the QR basis generation routine. As a result, the QR-decomposition has been called on a reduced snapshot matrix, and the offline stage has been significantly scaled down, in terms of central processing unit time.

Keywords Reduced-order method, Circuit analysis, Model order reduction, Numerical linear algebra

Paper type Research paper

This work is supported in parts by the Deutsche Forschungsgemeinschaft under grant no. CL143/18-1 and by the European Union's Horizon 2020 research and innovation programme under the Marie Skłodowska-Curie grant agreement no. 765374.

COMPEL - The international journal for computation and mathematics in electrical and electronic engineering

0332-1649
DOI 10.1108/COMPEL-02-2021-0050

1. Introduction

In manufacturing integrated circuits, a range of design explorations that ensure sound functionality of these components need to be performed. To this end, mathematical models of such circuits are simulated numerically. In a discrete setting, the required simulation times may become prohibitively large, in particular, for large-scale problems. Model reduction strategies arose as a remedy to recover computational feasibility for such problems, in particular, when repetitive computations are required. Here, we apply the maximum entropy snapshot sampling (MESS) method (Kasolis and Clemens, 2020) to nonlinear circuit problems, as means to reduced basis model reduction. In this paper, two case studies are presented. In the first case study, the commonly used proper orthogonal decomposition (POD) basis is substituted for a MESS obtained basis in a standard Galerkin projection setting for differential algebraic systems. The comparison against the POD demonstrates the overall performance of the advocated MESS framework. In the second case study, the MESS model order reduction framework is incorporated into a reduced order multirate (ROMR) scheme (Bannenberg *et al.*, 2021), which is applied to a coupled nonlinear thermal-electric circuit. Furthermore, in the second test case, the MESS method is combined with a maximum likelihood estimation of the parameter that controls the degree of reduction.

2. Method description

2.1 Maximum entropy snapshot sampling

Let $X = (x_1, x_2, \ldots, x_n)$ be a finite sequence of numerically obtained states $x_j \in \mathbb{R}^m$ at time instances $t_j \in \mathbb{R}$, with $j \in \{1, 2, \ldots, n\}$, of a diode chain model. Provided the probability distribution p of these states, the second-order Rényi entropy of the sample X is as follows:

$$H_p^{(2)}(X) = -\log \sum_{j=1}^{n} p_j^2 = -\log \mathbb{E}_p(p), \tag{1}$$

where $p_j \equiv p(x_j)$ and $\mathbb{E}_p(p)$ is the expected value of the probability distribution p with respect to p itself (Kasolis and Clemens, 2020). According to the law of large numbers, in the limit $n \to \infty$, the average of $p_1, p_2, \ldots, p_n$ almost surely converges to their expected value, that is:

$$\frac{1}{n} \sum_{j=1}^{n} p_j \to \mathbb{E}_p(p) \quad \text{as } n \to \infty, \tag{2}$$

while each p_j can be approximated by the sample's relative frequency of occurrence. By considering a norm $\| * \|$ on $\mathbb{R}^m$, the notion of occurrence can be translated into a proximity condition. In particular, for each $x_j \in \mathbb{R}^m$ define the open ball that is centred at x_j and whose radius is $\epsilon > 0$:

$$B_\epsilon(x_j) = \{y \in \mathbb{R}^m \,|\, \|x_j - y\| < \epsilon\}, \tag{3}$$

and introduce the characteristic function with values:

$$\chi_i(x_j) = \begin{cases} 1, & \text{if } x_j \in B_\epsilon(x_i), \\ 0, & \text{if } x_j \notin B_\epsilon(x_i). \end{cases} \tag{4}$$

Under the aforementioned considerations, the entropy of X can be estimated by:

$$\hat{H}_p^{(2)}(X) = -\log \frac{1}{n^2} \sum_{i=1}^{n} \sum_{j=1}^{n} \chi_i(x_j). \tag{5}$$

Provided that the limit of the evolution of $\hat{H}_p^{(2)}$ exists and measures the sensitivity of the evolution of the system itself (Broer and Takens, 2011, §6.6), a reduced sequence $X_\mathrm{r} = (x_{j_1}, x_{j_2}, \ldots, x_{j_r})$, with $r \leq n$, is sampled from X, by requiring that the entropy of X_r is a strictly increasing function of the index $k \in \{1,2,\ldots,r\}$ (Kasolis *et al.*, 2019). A reduced basis is then generated from X_r with any orthonormalization process. It has been shown (Kasolis and Clemens, 2020) that, depending on the recurrence properties of a system, any such basis guarantees that the Euclidean reconstruction error of each snapshot is bounded from above by ϵ, while a similar bound holds true for future snapshots, up to a specific time-horizon. See Algorithm 1 for the pseudo-code of the proposed method.

To estimate the parameter ϵ, which determines the degree of reduction within the MESS framework, the following optimisation approach is used (Takens, 1985). The quantity within the logarithm in the entropy estimate (5) is often referred to as the sample's correlation sum and can be written as follows:

$$C_\epsilon = \frac{1}{n^2} ||R_\epsilon||_\mathrm{F}^2, \tag{6}$$

with $R_\epsilon \in \{0,1\}^{n \times n}$ being the matrix whose entries are unity, when $||x_i - x_j|| < \epsilon$, and $|| * ||_\mathrm{F}^2$ being the Frobenius norm. In terms of probability theory, C_ϵ is a cumulative distribution function, and hence, its derivative $\mathrm{d}C_\epsilon/\mathrm{d}\epsilon$ is the associated probability density function. A commonly justified hypothesis is that the correlation sum scales as ϵ^D (Howell and Tong, 1993, Chapter 1), where $D \geq 0$ is the so-called correlation dimension of the manifold that is formed in $\mathbb{R}^m$ by the terms of X. Under this power law assumption, the maximum likelihood estimate (van der Waerden, 1969, Chapter 8) of the correlation dimension is estimated as follows. We find a sample $\{\epsilon_i\}$, with $\epsilon_i \in [0,1]$ for all $i \in \{1,2,\ldots,q\}$, of a random variable E that is distributed according to C_ϵ. Then, the probability of finding a sample in $(\epsilon_i, \epsilon_i + \mathrm{d}\epsilon_i)$ in a trial is as follows:

$$\prod_{i=1}^{q} D\epsilon^{D-1} \mathrm{d}\epsilon_i. \tag{7}$$

To calculate the ϵ value for which this expression is maximized, we take the logarithm:

$$q \cdot \ln D + (D-1) \sum_{i=1}^{q} \ln \epsilon_i, \tag{8}$$

and note that the maximum is attained when:

$$\frac{q}{D} + \sum_{i=1}^{q} \ln \epsilon_i = 0. \tag{9}$$

This results in the most likely value $\mathrm{D}_* = -1/\langle \ln E \rangle$, and ϵ can be estimated by:

$$\epsilon_* = \mathrm{argmin}(|D_* - \ln C_\epsilon / \ln \epsilon|). \tag{10}$$

Hence, MESS becomes a parameter-free method.

Algorithm 1: Maximum entropy snapshot sampling

input: Snapshot matrix $X \in \mathbb{R}^{m \times n}$, tolerance ϵ.
output: Reduced basis $V \in \mathbb{R}^{m \times r}$.

$P_{i,j} \leftarrow \|x_i - x_j\|, \forall i, j \in \{1, \ldots, n\}$;
$P \leftarrow P/\max(P)$;
$R \leftarrow P < \epsilon$;
$idx \leftarrow [1, 0, \ldots, 0] \in \{0,1\}^{1 \times n}$, $k \leftarrow 1$, $c \leftarrow 1$;
for $j = 1, 2, \ldots, n-1$ **do**
  $d_j = 2\sum_{k=1}^{j} R(j+1, k) + 1$;
  if $d - (2k+1)c < 0$ **then**
    $idx_{j+1} \leftarrow 1$;
    $c \leftarrow (k^2 c + d)/((k+1)^2)$;
    $k \leftarrow k + 1$;
  end
end
$[V, -] \leftarrow \mathrm{qr}(X(:, idx))$;

2.2 Reduced order multirate

The mathematical models that arise in the field integrated circuit simulation often encapsulate a plethora of hierarchical subsystems. These coupled subsystems often operate on different intrinsic time scales, which enables multirate time integration to have an advantageous effect (Günther *et al.*, 2001; Hachtel *et al.*, 2021). Multirate integration is especially effective if the slower subsystem is substantially larger, or more computationally expensive, than the faster subsystem. As the slow subsystems could still become prohibitively large, the multirate approach can be complemented with MOR techniques resulting in ROMR schemes.

When using a ROMR scheme (Bannenberg *et al.*, 2021), a semi-explicit differential-algebraic equation (DAE) is decomposed into fast and slow components, with subscripts F and S, respectively, for instance:

$$\dot{x_{\mathrm{F}}} = f_{\mathrm{F}}(x_{\mathrm{F}}, z_{\mathrm{F}}, x_{\mathrm{S}}), \qquad x_{\mathrm{F}}(0) = x_{\mathrm{F},0}, \tag{11}$$

$$\dot{x_{\mathrm{S}}} = f_{\mathrm{S}}(x_{\mathrm{F}}, z_{\mathrm{F}}, x_{\mathrm{S}}), \qquad x_{\mathrm{S}}(0) = x_{\mathrm{S},0}, \tag{12}$$

$$0 = g_{\mathrm{F}}(x_{\mathrm{F}}, z_{\mathrm{F}}, x_{\mathrm{S}}), \qquad z_{\mathrm{F}}(0) = z_{\mathrm{F},0}, \tag{13}$$

with f_{F}, f_{S} and g_{F} being known functions, and zero indexed quantities indicating known Cauchy data. Here, the fast and slow varying differential variables are $x_{\mathrm{F}} \in \mathbb{R}^{n_{\mathrm{F}}}$ and $x_{\mathrm{S}} \in \mathbb{R}^{n_{\mathrm{S}}}$, while the algebraic variable $z_{\mathrm{F}} \in \mathbb{R}^{n_{\mathrm{A}}}$ is assumed to be fast, because the dynamics of the DAE is considered to be fast in the time interval of interest. The described type of coupling enables the consideration of electrical circuits with a differential index up to unity, coupled to slower ODE systems.

To reduce the computational effort, a reduced basis that is to be used in a Galerkin projection framework is constructed. This reduction approach is then complemented with the gappy POD method (Willcox, 2006). By using a direct projection, the reduced system is

guaranteed to be again of unity index. To perform the reduction, let $V \in \mathbb{R}^{n_S \times r}$ be a non-square matrix whose columns constitute a reduced basis for the range of the slow varying states, with $n_S \gg r$. The full state x_S of the slow subsystem is then approximated by $x_S \cong V x_{S,r}$ using the reduced basis. Then, the reduced model becomes:

$$\dot{x}_F = f_F\left(x_F, z_F, V x_{S,r}\right), \quad x_F(0) = x_{F,0}, \tag{14}$$

$$\dot{x}_{S,r} = f_{S,r}\left(x_F, z_F, x_{S,r}\right), \quad x_{S,r}(0) = x_{S,r,0}, \tag{15}$$

$$0 = g_F\left(x_F, z_F, V x_{S,r}\right), \quad z_F(0) = z_{F,0}, \tag{16}$$

with $f_{S,r}\left(x_F, z_F, x_{S,r}\right) = V^\top f_S\left(x_F, z_F, V x_{S,r}\right)$, while the full state is needed for the coupling, and hence, again the gappy approach combined with a MESS basis is used.

The overall index one system (14)–(16) can be integrated with the L-stable implicit Euler scheme, which automatically assures that the algebraic constraints are not violated for all $t > 0$. To exploit the fast/slow decomposition, a multirate integration scheme has been proposed (Bannenberg *et al.*, 2021), which is a reduced order extension of a standard multirate scheme for DAEs (Hachtel *et al.*, 2021). The integration of the coupled system (14)–(16) for one macro-step $t_k \mapsto t_{k+1} = t_k + H$ can be written as follows:

$$x_{F,k+(\ell+1)/m} = x_{F,k+\ell/m} + h f_F\left(x_{F,k+(\ell+1)/m}, z_{F,k+(\ell+1)/m}, \overline{x}_{S,r,k+(\ell+1)/m}\right), \tag{17}$$

$$x_{S,r,k+1} = x_{S,r,k} + H f_{S,r}\left(\overline{x}_{F,k+1}, \overline{z}_{F,k+1}, x_{S,r,k+1}\right), \tag{18}$$

$$0 = g_F\left(x_{F,k+(\ell+1)/m}, z_{F,k+(\ell+1)/m}, \overline{x}_{S,r,k+(\ell+1)/m}\right), \tag{19}$$

where $\ell \in \{0, 1, \ldots, m-1\}$, $h = H/m$ is the micro-step size, and the coupling variables are denoted by $\overline{x}_F$, $\overline{z}_F$ and $\overline{x}_S$. Here, the coupling strategy is chosen to be the coupled-slowest-first, as this consistent for DAEs of unity order (Bannenberg *et al.*, 2021). First the system:

$$x^*_{F,k+1} = x_{F,k} + H f_F\left(x^*_{F,k+1}, z^*_{F,k+1}, x_{S,k+1}\right), \tag{20}$$

$$x_{S,r,k+1} = x_{S,r,k} + H f_{S,r}\left(x^*_{F,k+1}, z^*_{F,k+1}, x_{S,k+1}\right), \tag{21}$$

$$0 = g_F\left(x^*_{F,k+1}, z^*_{F,k+1}, x_{S,r,k+1}\right) \tag{22}$$

is solved for the macro-step. The step size H is chosen so that the solution to the slow subsystem remains sufficiently accurate. Then, the fast solutions $x^*_{F,k+1}$ and $z^*_{F,k+1}$ are not accurate enough and can be discarded, as they will be computed in the last micro-step. In the second stage, the fast solutions are computed for the micro-steps $\ell \in \{0, 1, \ldots, m-1\}$, using linear interpolation for the values $\overline{x}_{S,k+(\ell+1)/m}$, based on the available information $x_{S,k}$ and $x_{S,k+1}$.

3. Numerical experiments

3.1 Diode chain model

First, we will perform a case study regarding the sole application of the MESS reduction method to a diode chain. As an instance of an integrated circuit, consider the diode chain model that is depicted in Figure 1 and described by the differential-algebraic system (Verhoeven *et al.*, 2007):

$$\begin{aligned} &\Phi_1 - \Phi_{\text{in}}(t) = 0, \\ &I(\Phi_{i-1}, \Phi_i) - I(\Phi_i, \Phi_{i+1}) - \frac{\Phi_i}{R} - C\frac{\mathrm{d}\Phi_i}{\mathrm{d}t} = 0, \\ &I(\Phi_{m-2}, \Phi_{m-1}) - \frac{\Phi_{m-1}}{R} - C\frac{\mathrm{d}\Phi_{m-1}}{\mathrm{d}t} = 0, \\ &i_E - I(\Phi_1, \Phi_2) = 0, \end{aligned} \tag{23}$$

where $i \in \{2,3,\ldots m-2\}$ with integer $m > 3$, Φ_i is the voltage at the ith node of the circuit and is measured in V, while the time is measured in ns. The current–voltage diode characteristic function I: $\mathbb{R} \times \mathbb{R} \to \mathbb{R}$ is defined by:

$$I(x,y) = I_{\text{S}}[\mathrm{e}^{\alpha\cdot(x-y)} - 1], \tag{24}$$

where $I_{\text{S}} = 10^{-14}$ A is the saturation current and α is the inverse of the thermal voltage $\Phi_{\text{T}} = 0.0256$ V. Additional model parameters are mentioned in Figure 1. Further, the excitation voltage is as follows:

$$\Phi_{\text{in}} = \begin{cases} 20, & \text{if } t \leq 10, \\ 170 - 15t, & \text{if } 10 < t \leq 11, \\ 5, & \text{if } t > 11. \end{cases} \quad (\text{in V}) \tag{25}$$

To simulate a transient analysis of the diode chain model depicted in Figure 1, system (23) is integrated numerically. For large m such simulations become prohibitively expensive in terms of computational time. Here, to recover computational feasibility, reduced basis model reduction techniques are exploited. The MESS method is applied to the nonlinear diode chain model, with $m = 40{,}002$. The transient analysis is performed in the interval [0, 70] ns, using an implicit Euler scheme with time step $\Delta t = 0.1$ ns. Consistent initial conditions are obtained through a direct current simulation using very small time steps and using a linear increasing input voltage from $\Phi_{\text{in}} = 0$ to $\Phi_{\text{in}} = 20$. The reduced bases are generated from

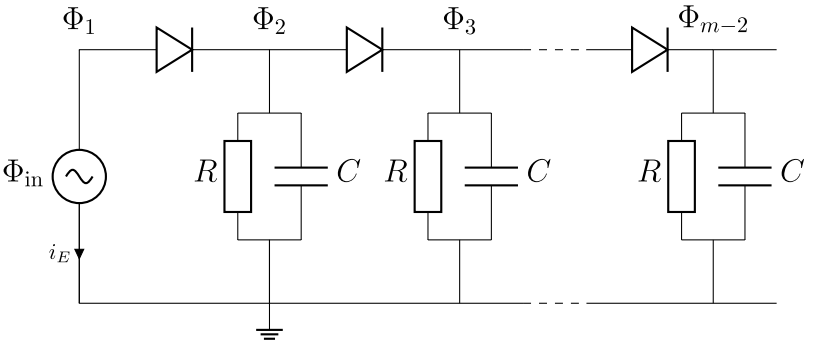

Figure 1.
Diode chain with $R = 10^4\,\Omega$ and $C = 10^{-12}$ F

the high-fidelity matrix $X \in \mathbb{R}^{m \times n}$, with $n = 701$ (Figure 2). To benchmark the presented MESS based reduction, a comparison with the POD method is made. The number of POD modes is taken to be equal to the number of MESS-obtained basis vectors. In the Newton iterations, least squares approximations by use of gappy POD, of the Jacobian matrix are used.

Here, the estimated ϵ_* value is equal to 0.00525. However, in an attempt to maximally reduce the studied system, ϵ is manually selected close to a value that turns out to yield a numerically unstable reduced model. In Figure 3, the case of the MESS reduced system for $\epsilon = 0.0325$ is depicted. There, it is shown that the solution to the MESS reduced system converges to the reference solution. To illustrate that some caution is needed if ϵ is selected

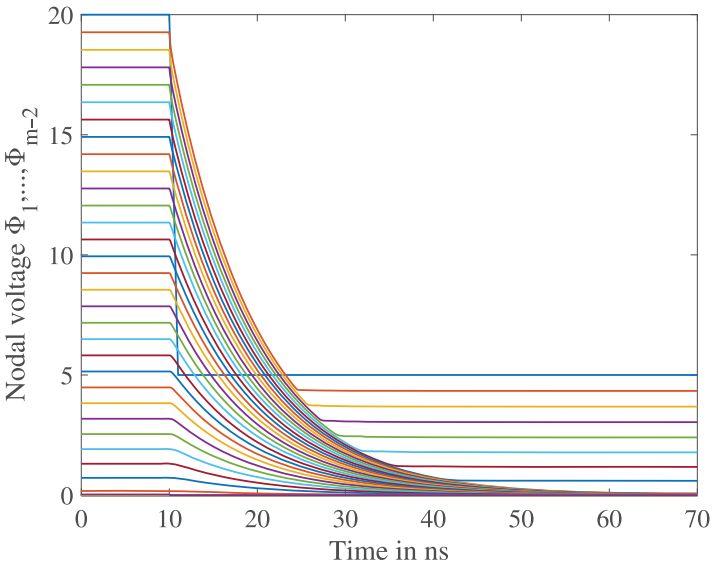

Figure 2.
Output of the transient analysis for all nodes

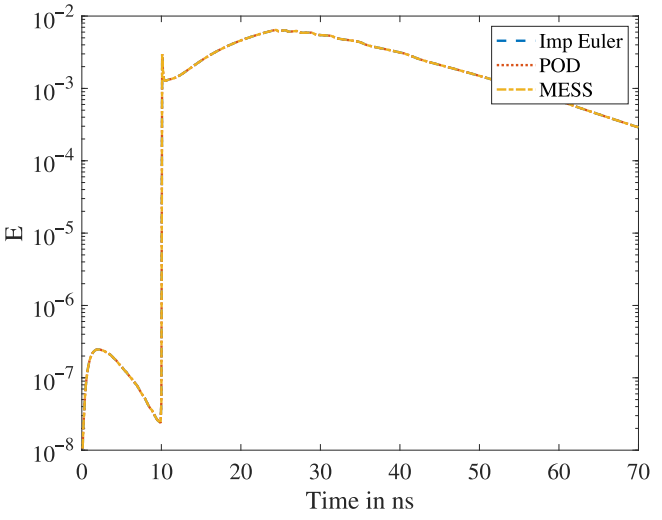

Figure 3.
Difference $E(t) = \| \Phi_{HF} - \Phi \| / \| \Phi_{HF} \|$ for the parameter value $\epsilon = 0.0325$. The subscript HF stands for "high-fidelity"

manually, in Figure 4, a slightly higher ϵ value is chosen, when the resulting reduced model becomes unstable. In Table 1, the computational times that are required for generating the bases suggest that the MESS has an advantage in the offline stage. Further, for large-scale problems, the singular value decomposition becomes infeasible because of memory constraints, whereas this is not the case for MESS, because it relies on recursive evaluations.

3.2 Thermal-electric circuit

As the ROMR case study circuit needs to contain both coupling and different intrinsic time scales, a thermal-electric test circuit is used (Bartel *et al.*, 2003). This circuit consists of an operational amplifier, two resistors, a diode and a capacitor. The thermal resistor $R(T)$ is modelled by a structure of length $d = 0.03$ m and variable diameter $a(x) = a_0/[1 + b(d - x)x]$, with $x \in [0,d]$, while the material parameters are those of a copper wire. The local resistance:

$$\rho(T) = r_0\left(1 + \alpha(T - T_{\text{meas}}) + \beta(T - T_{\text{meas}})^2\right) \tag{26}$$

exhibits quadratic dependence on the temperature. The local resistance per unit cross section is thus expressed in Ω m. Using this expression, the total resistance of the wire is as follows:

$$R(T) = \int_0^d \rho\left(\frac{\xi, T(t, \xi)}{a(\xi)\mathrm{d}\xi}.\right. \tag{27}$$

Electrical parameters of one-dimensional resistor

Material	Cu (copper)
Specific resistance	$r_0 = 1.7\ \mu\Omega$ m
Reference temperature	$T_{\text{meas}} = 291$ K
Length	$d = 0.03$ m
Cross section	$a_0 = 540$ m
Profile	$b = (2/d)^2$ m^2
1st thermal coefficient	$\alpha = 1/(273\,\text{K})$
2nd thermal coefficient	$\beta = 1/(273\,\text{K})^2$

Thermal parameters of the one-dimensional resistor

Density	$d_{\text{w}} = 8.9810^3$ kg/m^3
Heat conductivity	$\lambda_{\text{w}} = 390$ W/(mK)
Specific heat	$c_{\text{w}} = 385$ J/(kg K)
Transition coefficient	$\gamma = 1.0$ W/(m^2 K)
Thermal mass	$M'_{\text{w},i} = a(x_i)d_{\text{w}}c_{\text{w}}$ J/K
Cooling surface	$S'_{\text{w},i}(x) = 2\sqrt{\pi a(x)}$

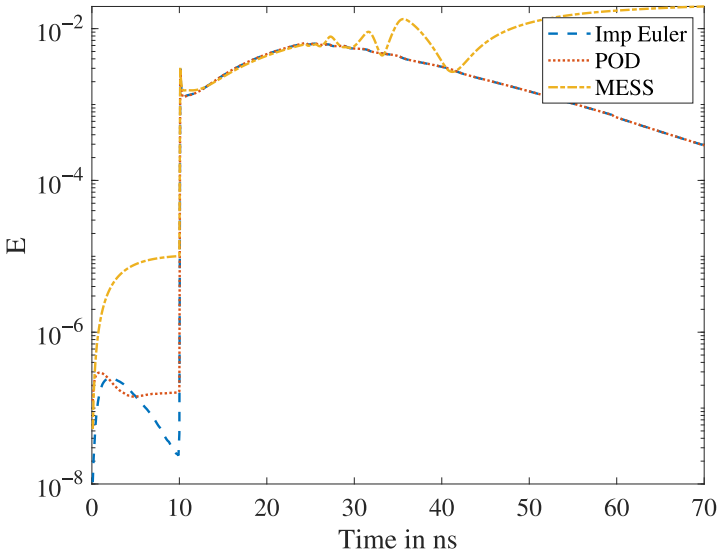

Figure 4. Difference $E(t) = \| \Phi_{HF} - \Phi \| / \| \Phi_{HF} \|$ for the parameter value $\epsilon = 0.0425$

	$\epsilon = 0.0325$		$\epsilon = 0.0425$	
	Basis generation	m	Basis generation	m
High-fidelity		40,002		40,002
POD	1.5400 s	31	1.3397 s	25
MESS	0.1733 s	31	01577 s	25

Table 1. Timing MESS vs POD (time in seconds)

The amplifier is a heat source and the diode has a temperature-dependent characteristic i_{di} (u_{di}, T_{di}) curve:

$$i_{di}(u_{di}, T_{di}) = \hat{I}_S(T_{di}) \left[e^{\frac{u_{di}}{v_T}} - 1 \right], \tag{28}$$

$$\hat{I}_S(T_{di}) = 10^{-12} \left(\frac{T_{di}}{300\text{K}} \right)^3 e^{\frac{-qE_g(300\text{K})}{k_B T_{di}} \left(1 - \frac{T_{di}}{300\text{K}}\right)}. \tag{29}$$

Electrical parameters of the zero-dimensional elements

Specific resistance	$q = 1.602 \times 10^{-19}$ C
Energy gap	$E_g(300\text{ K}) = 1.11$ V
Boltzmann constant	$k_B = 1.38110^{-23}$ J/K
Thermal voltage	$v_T = k_B\, T_{di}/q$ V
Operational power	$v_{op} = 15$ V
Amplification	$A = 20{,}000$
Load resistance	$R_L = 0.3$ kΩ
Capacitance	$C = 500$ nF

The electric behaviour of the circuit is modelled by modified nodal analysis based on Kirchhoff's laws. The thermal model is nonlinear because of the coupling terms, where the local self-heating term, P_w, introduces the nonlinear terms. After discretizing in space, the following thermal-electric system is obtained.

Electric network

$$0 = (Av(t) - u_3)/R(T) + i_{di}(u_3 - u_4, T_{di}),$$
$$C\dot{u}_4 = i_{di}(u_3 - u_4, T_{di}) - u_4/R_L,$$

Coupling interfaces

$$P_{op} = |(v_{op} - |v(t)|) \cdot (Av(t) - u_3)/R|, \qquad P_w = (Av(t) - u_3)^2/R,$$

$$R(T) = \left(\frac{1}{2}\left(\rho(0, T_0) + \sum_{i=1}^{N-1}\rho(X_i, T_i) + \frac{1}{2}\rho(l, T_N)\right) \cdot h,\right.$$

Heat equation

$$M'_{w,i}h\dot{T}_i, = \Lambda\frac{T_{i+1} - 2T_i + T_{i-1}}{h} + P_w\frac{\tilde{\rho}(X_i, T_i)}{R}h - \gamma S'_{w,i}h(T_i - T_{env}), (i = 1, \ldots, N-1),$$

$$\left(M'_{w,0} \cdot \frac{h}{2} + M_{op}\right)\dot{T}_0 = \Lambda\frac{T_1 - T_0}{h} + P_w\frac{\tilde{\rho}(0, T_0)}{R}\frac{h}{2} - \gamma\left(S'_{w,0}\frac{h}{2} + S_{op}\right) \cdot (T_0 - T_{env}) + P_{op},$$

$$\left(M'_{w,N} \cdot \frac{h}{2} + M_{di}\right)\dot{T}_N = \Lambda\frac{T_{N-1} - T_N}{h} + P_w\frac{\tilde{\rho}(X_N, T_N)}{R}\frac{h}{2} - \gamma\left(S'_{w,N}\frac{h}{2} + S_{di}\right) \cdot (T_N - T_{env})$$

Extension parameters of the zero-dimensional elements

Amplifier	cubic
Material	Al (aluminium)
Size	$e_{op} = 0.5$ mm
Heat capacity	$c_{Al} = 449$ J/(kg K)
Density	$d_{al} = 2.710^3$ kg/m^3
Cooling surface	$S_{op} = 6 \cdot e_{op}^2$ mm^2
Diode	cubic
Material	Si (silicon)
Size	$e_{di} = 0.167$ mm
Heat capacity	$c_{Al} = 700$ J/(kg K)
Density	$d_{si} = 2.3310^3$ kg/m^3
Cooling surface	$S_{di} = 6 \cdot e_{di}^2$ mm^2

The computational cost of coupled network simulations is reduced by applying the ROMR scheme. Here, multirate integration and the MESS are used for solving the equations that govern the thermal-electric circuit that is depicted in Figure 5. After partitioning the slow and fast varying timescales, problem (14)–(16) becomes:

$$\begin{aligned} \dot{x}_{\mathrm{F}} &= f_{\mathrm{F}}\left(x_{\mathrm{F}}, z_{\mathrm{F}}, Vx_{\mathrm{S,r}}\right), & x_{\mathrm{F}}(0) &= x_{\mathrm{F},0}, \\ \dot{x}_{\mathrm{S,r}} &= f_{\mathrm{S,r}}\left(x_{\mathrm{F}}, z_{\mathrm{F}}, x_{\mathrm{S,r}}\right), & x_{\mathrm{S,r}}(0) &= x_{\mathrm{S,r},0}, \\ 0 &= g_{\mathrm{F}}\left(x_{\mathrm{F}}, z_{\mathrm{F}}, Vx_{\mathrm{S,r}}\right), & z_{\mathrm{F}}(0) &= z_{\mathrm{F},0}. \end{aligned} \tag{30}$$

Here, $x_{\mathrm{F}} = u_4$, $z_{\mathrm{F}} = u_3$ and $x_{\mathrm{S,r}} = V^{\top} x_{\mathrm{S}}$, with $x_{\mathrm{S}} \in \mathbb{R}^m$ being the discretized temperature in the thermal resistor (Figure 6).

Problem (30) is integrated with a ROMR method, and the parameter ϵ is computed by (10) (Figure 7). To verify the performance of (ROMR, MESS, ϵ_*), a transient analysis for the output u_4 is performed. A reference solution is obtained with a standard multirate scheme of five fine-grid steps for a problem with $(m, n) = (10^4, 500)$. Then, the ROMR scheme is used, once with (MESS, ϵ_*) and once with the POD. In Figure 7, both the correlation sum (left) and an accuracy plot (right) for (MESS, 0.0816) are depicted. The accuracy result for the POD is indistinguishable from the one depicted in Figure 7 (right), and hence, it is omitted. The degrees of freedom are reduced from 10^4 to 13, while the optimal ϵ_* is estimated in 2.9 s and the MESS base is constructed in 0.16 s, in contrast to a total of 6.33 s that is required by the POD.

4. Conclusions

The MESS has been successfully used for reducing two nonlinear circuits: in particular, a diode chain model and a thermal-electric coupled system. In both cases, the MESS removed

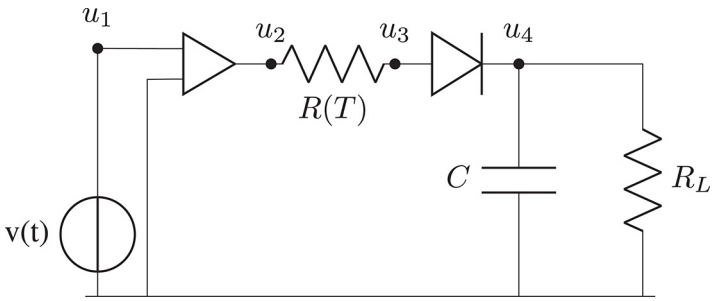

Figure 5.
Circuit used for the numerical experiments

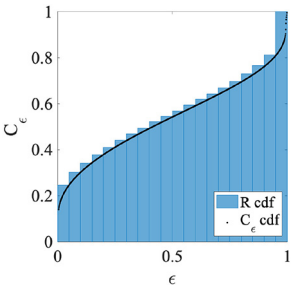

Figure 6.
Cumulative distribution (cdf) of R and C_ϵ

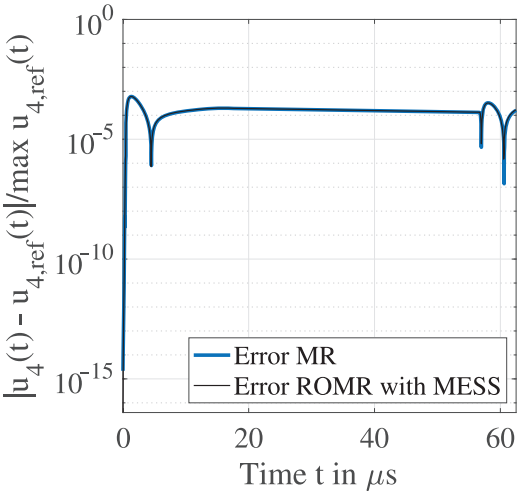

Figure 7.
Relative difference between standard multirate and ROMR with (MESS, 0.0816)

unnecessary data, and hence, it reduced the snapshot matrix, before calling the QR basis generation routine. As a result, the triangular-orthogonal decomposition has been called on a reduced snapshot matrix, and the offline stage has been significantly scaled down, in terms of central processing unit (CPU) time. Because the MESS relies on pairwise distance computations, its performance can be further improved through CPU/graphics processing unit parallelization, while it enables an accept/reject routine that can be incorporated into the high-fidelity solver, to immediately decide whether or not a new snapshot needs to be stored. This last feature reduces storage requirements, while, to our knowledge, the MESS is the only black-boxed method for performing non-homogeneous snapshot sampling, without relying on prior knowledge regarding the application at hand. Through the optimality requirement for selecting the parameter ϵ, the MESS does not require any user input, and hence, it can be seen as a parameter-free method, while a single parameter is required in general. Further research needs to be conducted for selecting an ϵ value that guarantees stability and maximally reduced models. The obtained bases have been used in a gappy framework for reduced nonlinear function evaluation, while the corresponding reduced models perform as accurate as the standard reduction framework that relies on the singular value decomposition.

References

Bannenberg, M.W.F.M., Ciccazzo, A. and Günther, M. (2021), "Coupling of model order reduction and multirate techniques for coupled dynamical systems", *Applied Mathematics Letters*, Vol. 112, p. 106780, doi: 10.1016/j.aml.2020.106780, available at: www.sciencedirect.com/science/article/pii/S0893965920303967

Bartel, A., Günther, M. and Schulz, M. (2003), "Modeling and discretization of a thermal-electric test circuit", *In Modeling, Simulation, and Optimization of Integrated Circuits*, Springer, New York, NY, pp. 187-201.

Broer, H. and Takens, F. (2011), *Dynamical Systems and Chaos*, Springer-Verlag, New York, NY.

Günther, M., Kvaernø, A. and Rentrop, P. (2001), "Multirate partitioned Runge-Kutta methods", *BIT Numerical Mathematics*, Vol. 41 No. 3, pp. 504-514.

Hachtel, C., Bartel, A., Günther, M. and Sandu, A. (2021), "Multirate implicit Euler schemes for a class of differential–algebraic equations of index-1", *Journal of Computational and Applied Mathematics*, Vol. 387, p. 112499, doi: 10.1016/j.cam.2019.112499, available at: www.sciencedirect.com/science/article/pii/S0377042719305023

Howell, A. and Tong, M. (1993), *Dimension Estimation and Models*, World Scientific, Vol. 1.

Kasolis, F. and Clemens, M. (2020), "Maximum entropy snapshot sampling for reduced basis generation", arXiv preprint arXiv:2005.01280.

Kasolis, F., Zhang, D. and Clemens, M. (2019), "Recurrent quantification analysis for model reduction of nonlinear transient electro-quasistatic field problems", *In International Conference on Electromagnetics in Advanced Applications (ICEAA 2019)*, pp. 14-17.

Takens, F. (1985), "On the numerical determination of the dimension of an attractor", *In Dynamical Systems and Bifurcations*, Springer, New York, NY, pp. 99-106.

van der Waerden, B.L. (1969), *Mathematical Statistics*, Springer, New York, NY.

Verhoeven, A., Ter Maten, J., Striebel, M. and Mattheij, R. (2007), "Model order reduction for nonlinear IC models", *In IFIP Conference on System Modeling and Optimization*, Springer, New York, NY, pp. 476-491.

Willcox, K. (2006), "Unsteady flow sensing and estimation via the gappy proper orthogonal decomposition", *Computers and Fluids*, Vol. 35 No. 2, pp. 208-226.

Corresponding author
Marcus W.F.M. Bannenberg can be contacted at: bannenberg@uni-wuppertal.de